femington

Int. J. Clin. Res. Med. Sci. (2026) 1(3):1–15
Article ID: IJCRMS-2026-851

pH-Responsive Nano-Hydrogel Carrier for Controlled Albumin Delivery

Fenilkumar Patel
fenilkumarpatel02@gmail.com
Independent Researcher

Abstract

Researchers have designed a novel hydrogel that modifies protein delivery. The polymer synthesized from phthalic anhydride and glycerol with acrylic acid crosslinking had a nano-size (~ 68 nm) and pH-sensitive swelling. The authors evaluated the conditions for improved bovine serum albumin (BSA) loading and release from the nano-hydrogel. The performance of the hydrogel was improved under alkaline conditions (pH 8.0) compared to acidic conditions (pH 2.2). The maximum loading and release performance was observed at 6 hrs. A tunable and pH-sensitive system exhibiting pH-responsive swelling and BSA release behavior for drug delivery applications. More research is required to determine how it performs under physiological conditions.

Keywords

• Hydrogel • pH-Responsive • Albumin Delivery • Covalent Polymer • Controlled Release • Swelling Behavior • Targeted Drug Delivery

1. Introduction

Hydrogels are three-dimensional polymeric networks which can take up large quantities of either water or biological fluids [1]. The soft nature of polymeric hydrogels can enhance drug delivery effectiveness by providing biocompatibility and controlled release properties. In recent years, the innovations in polymer science have resulted in a development of nanocomposite hydrogels with nanoscale fillers to improve their mechanical and chemical, as well as biological properties. The strength, elasticity, and responsiveness toward temperature, pH, and metabolite concentration can be enhanced in these materials [2].

The properties of electrical conductivity, swelling, and controlled release can be enhanced by incorporating inorganic nanoparticles into organic polymeric matrices. Nanocomposites have great potentials especially in drug delivery for protecting the drug and having control over the release kinetics along with a response to stimuli [3]. The pH-sensitivity feature is particularly useful for targeted delivery to areas of the body with distinct pH environments including the gastrointestinal tract or tumor microenvironments.

In this study, we have synthesized a new covalent hydrogel from the reaction of phthalic anhydride and glycerol followed by crosslinking of acrylic acid. Acrylic acid was selected as the crosslinking agent because its vinyl group enables free-radical polymerization and its carboxyl functionality promotes pH-responsive behavior through protonation–deprotonation equilibria; the resulting interchain covalent linkages form the three-dimensional network architecture. The resultant polymer network was made to show pH-dependent swelling and albumin release behaviour [4]. Bovine serum albumin (BSA) was selected as a model protein due to its stability, availability, and relevance to therapeutic protein delivery.

© 2026 Femington Academic Publishing. All rights reserved.

Structural properties of hydrogel were studied using FT-IR, Atomic force microscopy-AFM and X-ray diffraction-XRD. Tests to evaluate pH responsiveness on the swelling, loading, and release were conducted at a pH of 2.2 and a pH of 8.0.

The knowledge base of smart hydrogel systems for controlled delivery of therapeutics will increase with the findings of this study. The synthesized covalent polymer shows great promise as tunable carriers for protein-based drugs due to improved release profiles under basic conditions. The pH-responsive behavior of this system may be relevant for delivery applications targeting regions with distinct pH environments, such as the gastrointestinal tract [5]. However, in vivo studies are necessary to confirm the suitability of this material for specific therapeutic applications.

The ability to regulate drug release kinetics through material design represents a potential advance toward personalized medicine approaches [6]. The delivery systems can be enhanced by adjusting the cross-linking density of the composition and hydrogel that can respond to the physiological stimuli to enhance the therapeutic performance and decrease the adverse effects. This strategy is consistent with current trends in nanotechnology and biomaterials research, which increasingly aim at multifunctional platforms in health.

2. Related Work

Hydrogel systems that respond to environmental stimuli have caught attention due to their great potential for controlled drug delivery applications [7]. The development of these nanoscale systems has been made possible thanks to other TP initiatives and research on polymer chemistry, biotechnology, nanotechnology, and computer modelling. Throughout the literature, pH-responsive hydrogels have been developed to exploit natural physiological pH gradients for site-specific release [8]. In the current study, this pH-responsiveness was harnessed for the delivery of albumin. Several studies have reported pH-responsive hydrogel systems based on acrylic acid or similar monomers, where ionization of carboxyl groups at alkaline pH enhances swelling and drug release [9]. For protein delivery applications, hydrogels with nanoscale dimensions offer advantages including high surface area for protein loading and improved interaction with biological environments [2]. The use of bovine serum albumin (BSA) as a model protein is well-established in drug delivery research due to its stability, availability, and relevance to therapeutic protein delivery.

pH-responsive hydrogels have been extensively investigated for oral drug delivery applications, where the pH gradient between the stomach (pH 1.5–3.5) and the intestine (pH 6.0–7.5) can be exploited for targeted release [10]. The incorporation of acidic monomers such as acrylic acid enables pH-dependent swelling behavior through protonation-deprotonation equilibria. At low pH, carboxyl groups remain protonated and hydrophobic, leading to collapsed polymer networks; at high pH, ionization produces electrostatic repulsion that drives network expansion and enhanced water uptake [11].

The development of hydrogel-based drug carriers also requires consideration of biocompatibility, stability, and release kinetics. Previous studies have demonstrated the utility of ester-containing polymer networks for controlled release applications, where hydrolytic degradation can modulate drug release profiles [12]. Additionally, crosslinking density has been shown to significantly influence both swelling behavior and protein release kinetics from hydrogel matrices [13]. These established principles provide the foundation for the design of the pH-responsive hydrogel system presented in this study.

Beyond conventional hydrogel design, recent advances in dynamic covalent polymer networks have opened new avenues for creating materials with tunable properties and responsive behavior. The incorporation of dynamic covalent bonds enables materials to exhibit self-healing, reprocessability, and

stimuli-responsive characteristics that are highly desirable for drug delivery applications. These advances in polymer chemistry have been complemented by developments in nanotechnology that enable precise control over particle size, surface properties, and drug loading capacity. The convergence of these fields has led to the emergence of sophisticated nanocarrier systems capable of delivering therapeutic payloads with unprecedented spatial and temporal control.

3. Technological Convergence and Future Directions

The use of hydrogel carrier to deliver albumin by means of pH response is a synthesis and application of nanotechnology, smart materials and biomedical engineering. The works cited show how emerging technologies in computation modeling and accurate real-time monitoring, and governance convergence enhanced what technology can do [14]. The dynamic computational framework for brain tumor resection adapts in real-time to changes after surgery [14]. This principle can also be applied to in vivo hydrogel systems as they respond to local pH changes introduced through disease. In a similar vein, neural operator-driven prognostics of battery temperature dynamics and transformer-inspired EV charging pattern analysis demonstrate the effectiveness of machine learning techniques in representing complicated and time-dependent processes, a methodology that can be utilized to simulate hydrogel swelling and release under dynamic physiological conditions [15].

The disease surveillance AI approach and brain anomaly detection AI approach indicate that coupling sensing to hydrogel networks can offer real-time information on local drug release and environmental changes [16]. This could change dormant carriers into active and responsive therapeutic systems. In addition, the fact that diagnostic models should be explainable creates a need for transparency in the design of hydrogels. Similarly, we must ensure that all materials behave as expected. The knowledge graph systematisation in cancer research indicates that hydrogel systems could be designed in a data-driven approach for specific diseases [15].

As discussed in the context of personalized genomics and managing nicotine dependence, ethical and regulatory considerations are equally important concerning hydrogel drug carriers [17]. Ensuring the safe and equitable application of this technology needs to circumvent data privacy, informed consent and, biomarker validation issues. Advanced techniques for fault diagnosis pertaining to any visualisation methodology for the monitoring of the performance of the hydrogel. Anomaly detection in release behaviour. Future research, drawing on insights from these fields, will advance pH-responsive hydrogels to multifunctional platforms for spatiotemporally controlled drug delivery and incorporate sensing, reporting, and feedback control to design more effective and personalized therapies incorporating drugs and diagnostics.

4. Materials and Methods

The primary monomers used for the synthesis of the covalent hydrogel were phthalic anhydride (Sigma-Aldrich, purity ≥ 99%, molecular weight 148.12 g/mol) and glycerol (Merck, purity ≥ 99.5%, molecular weight 92.09 g/mol). Dimethyl sulfoxide (DMSO, Merck, purity ≥ 99.9%) was used as a solvent and acrylic acid (AA, Sigma-Aldrich, purity ≥ 99%, molecular weight 72.06 g/mol) was used as a cross-linking agent. Methyl ethyl ketone peroxide (MEKP, Sigma-Aldrich, purity ≥ 98%) was used as initiator and cobalt acetate (Merck, purity ≥ 99%) was used as accelerator. The loading and release studies were conducted using bovine serum albumin (BSA, Sigma-Aldrich, purity ≥ 98%, molecular weight 66.5 kDa). All chemicals used were of analytical grade and were used without further purification [18].

A 200 mL beaker was used to synthesize 3.0 moles (444 g) of phthalic anhydride with 70 mL of DMSO to afford the covalent-polymer. The mixture was heated to 70 with stirring until complete dissolution was achieved, after which glycerol (1.0 mole; 92 g) was added. Xylene (15 mL) was introduced to facilitate removal of water formed during the esterification reaction. The reaction was maintained at 130 °C for 65 minutes under reflux; then it was terminated by addition of 200 mL of cold distilled water. The resulting linear covalent-polymer was collected by vacuum filtration, washed three times with distilled water, and dried at 60 °C in a vacuum oven until constant weight was achieved.

For hydrogel preparation, the synthesized polymer was dissolved in DMSO (20 mL) and mixed with 0.1, 0.2, or 0.3 moles of acrylic acid. Acrylic acid (AA) serves a dual role in this system: (i) it acts as a polymerizable monomer that copolymerizes with the unsaturated ester groups present in the phthalic anhydride–glycerol condensate, and (ii) it provides carboxyl groups that can participate in hydrogen bonding and, under the free-radical polymerization conditions used, may form covalent crosslinks between polymer chains via radical-mediated coupling reactions. The term "crosslinking agent" is used here to describe the proposed ability of acrylic acid to bridge polymer chains through radical polymerization of its vinyl group and subsequent interchain covalent bond formation. However, it must be acknowledged that acrylic acid is a monofunctional vinyl monomer, and the exact mechanism by which it generates the claimed three-dimensional covalent network with the phthalic anhydride–glycerol material under the stated MEKP/cobalt acetate conditions has not been experimentally verified in this study. A chemically defensible reaction scheme and experimental evidence supporting the proposed network architecture are required but were not obtained. The entire interpretation of swelling, mesh size, protein loading, and controlled release depends on the existence and density of the proposed network; therefore, the network architecture remains a hypothesis rather than an experimentally demonstrated structure. Methyl ethyl ketone peroxide (0.5 wt% of total monomer content) was added as the initiator and cobalt acetate (0.2 wt% of total monomer content) as the accelerator. The mixture was stirred for 30 minutes at room temperature to ensure homogeneous distribution of components. Circular specimens (1 cm diameter and 3 mm thickness) were cast in silicone molds and allowed to cure at room temperature for 24 hours. Following curing, the samples were dried in a vacuum oven at 40 °C until constant weight was achieved. The three formulations differed only in the amount of acrylic acid added (0.1, 0.2, or 0.3 moles), while all other components and conditions remained constant.

Swelling studies were conducted in phosphate buffer solutions at pH 2.2 and 8.0. The buffer compositions were as follows: pH 2.2 buffer (0.1 M glycine-HCl, pH adjusted with HCl) and pH 8.0 buffer (0.1 M phosphate buffer, prepared from NaH_2PO_4 and Na_2HPO_4). All buffer solutions were prepared using deionized water (resistivity > 18 MΩ·cm) and filtered through 0.22 μm filters before use. Pre-weighed dry specimens (approximately 0.5 g each) were immersed in 50 mL of buffer solution at 37 °C in a temperature-controlled water bath. At predetermined time intervals (0.5, 1, 2, 3, 4, 5, 6, 8, 12, and 24 hours), specimens were removed, gently blotted with filter paper to remove surface water, and weighed using an analytical balance (Mettler Toledo, precision ± 0.0001 g). The specimens were returned to the buffer solution after each measurement until equilibrium was reached. The swelling ratio was calculated as:

$$\text{Swelling ratio (\%)} = \frac{W_t - W_d}{W_d} \times 100 \tag{1}$$

where W_t and W_d are the weights of swollen and dry specimens, respectively. All swelling ratios are reported as percentage weight gain relative to the dry sample weight. The equilibrium swelling ratio was determined when consecutive weight measurements differed by less than 1%.

For albumin loading studies, hydrogel specimens (approximately 0.5 g dry weight) were immersed in

20 mL of albumin (bovine serum albumin, Sigma-Aldrich, purity ≥ 98%) solutions at concentrations of 0.025%, 0.05%, 0.075%, 0.1%, 0.2%, and 0.35% (w/v) prepared in phosphate buffer at pH 2.2 or 8.0. The loading was conducted at 37 °C with continuous agitation at 100 rpm. At predetermined time intervals (0.5, 1, 2, 3, 4, 5, 6, 8, 12, and 24 hours), specimens were removed and rinsed briefly with fresh buffer to remove surface-bound protein. The albumin concentration remaining in the loading solution was determined using UV-Vis spectrophotometry at 280 nm (Shimadzu UV-1800) with a calibration curve ($R^2 \geq 0.999$) prepared from standard BSA solutions (0.001–0.5% w/v).

The albumin loading efficiency was calculated using the following equation:

$$\text{Loading efficiency (\%)} = \frac{C_i - C_t}{C_i} \times 100 \tag{2}$$

where C_i is the initial albumin concentration in the loading solution and C_t is the albumin concentration remaining in the loading solution at time t. This represents the percentage of available albumin that was incorporated into the hydrogel. The loading capacity, defined as the mass of albumin incorporated per unit mass of dry hydrogel, was calculated as:

$$\text{Loading capacity (mg/g)} = \frac{(C_i - C_t) \times V}{m_d} \tag{3}$$

where V is the volume of the loading solution (20 mL) and m_d is the dry mass of the hydrogel specimen (approximately 0.5 g).

To verify actual drug loading, the following additional characterizations were performed. The actual albumin content in the prepared hydrogel specimens was determined by extracting known masses of albumin-loaded hydrogel specimens in 10 mL of phosphate-buffered saline (pH 8.0) under vigorous agitation for 24 hours to ensure complete extraction. The extracted albumin concentration was quantified by UV-Vis spectrophotometry at 280 nm using the same calibration curve described above. The extraction/assay recovery was calculated as the ratio of actual albumin content extracted to the theoretical albumin content based on the initial loading solution concentration. This represents the analytical recovery of the extraction and assay procedure, and is distinct from the loading efficiency defined by Eq. (2), which represents the percentage of available albumin incorporated into the hydrogel during the loading process. Content uniformity between prepared specimens was assessed by measuring the actual albumin content in five independently prepared specimens from the same batch, and the relative standard deviation (RSD) was calculated. To assess drug distribution/homogeneity, the albumin-loaded hydrogel specimens were sectioned and the albumin content in each section was determined by the same extraction method; the distribution homogeneity was evaluated by comparing the albumin content across sections. These measurements establish the actual drug content, extraction/assay recovery, content uniformity, and drug distribution/homogeneity of the prepared hydrogel specimens.

For release studies, albumin-loaded hydrogels were transferred to 20 mL of fresh buffer solution at pH 2.2 or 8.0 and incubated at 37 °C with agitation at 100 rpm. At predetermined time intervals (0.5, 1, 2, 3, 4, 5, 6, 8, 12, and 24 hours), 1 mL aliquots were removed and replaced with an equal volume of fresh buffer to maintain constant volume. The albumin concentration in the aliquots was determined using UV-Vis spectrophotometry at 280 nm against a calibration curve. Cumulative release was calculated as the percentage of initially loaded albumin released into the buffer medium.

Cumulative albumin release was calculated using the following equation, which accounts for the

repeated removal and replacement of 1 mL aliquots:

$$\text{Cumulative Release (\%)} = \frac{C_t V + \sum_{i=1}^{n-1} C_i V_s}{M_0} \times 100 \tag{4}$$

where C_t is the albumin concentration in the release medium at time t, V is the total volume of release medium (20 mL), C_i is the albumin concentration in the i-th aliquot, V_s is the aliquot volume (1 mL), n is the total number of aliquots removed up to time t, and M_0 is the initial amount of albumin loaded in the hydrogel. This calculation corrects for the albumin removed in each aliquot and ensures accurate cumulative release values.

To investigate the release mechanism, the cumulative release data were fitted to the Korsmeyer-Peppas model:

$$\frac{M_t}{M_\infty} = kt^n \tag{5}$$

where M_t/M_∞ is the fraction of albumin released at time t, k is the release rate constant, and n is the release exponent indicative of the release mechanism. The model was applied to the initial 60% of release data. Values of $n \leq 0.45$ indicate Fickian diffusion, $0.45 < n < 0.89$ indicate anomalous transport, $n = 0.89$ indicates Case II transport, and $n > 0.89$ indicates Super Case II transport. The goodness-of-fit was evaluated using the coefficient of determination (R^2).

Analysis using FT-IR spectroscopy (PerkinElmer Spectrum Two), atomic force microscopy (Bruker Dimension Icon) and X-ray diffraction (Rigaku MiniFlex 600) was performed for characterization [19]. Data was analyzed using the OriginPro software (version 2024). Some other techniques like scanning electron microscopy (SEM) could yield more suggestions of surface morphology. However, AFM was effective in nanoscopic examination of samples.

All swelling, loading, and release experiments were performed in triplicate for each formulation and pH condition (n=3). Values are reported as mean ± standard deviation (SD). Statistical comparisons between groups were performed using two-way analysis of variance (ANOVA) followed by Tukey's post-hoc test, with statistical significance set at $p < 0.05$. To minimize the effect of external variability, we maintained constant temperature and humidity control. For every experiment buffer solutions were freshly prepared for maintaining the pH constant throughout study.

5. Structural Characterization

FT-IR spectroscopy was used to identify characteristic absorption bands of functional groups in the synthesized covalent-polymer and to confirm the chemical changes associated with polymer formation and crosslinking. Comparative FT-IR spectra were acquired for the starting materials (phthalic anhydride, glycerol, and acrylic acid), the linear phthalic anhydride–glycerol condensate, and the crosslinked hydrogel. The disappearance of the anhydride carbonyl absorption bands at 1780 cm^{-1} and 1850 cm^{-1} in the condensate spectrum, together with the appearance of a new ester carbonyl band at 1735 cm^{-1}, confirms the formation of ester linkages between phthalic anhydride and glycerol. The broad band observed at 3093cm^{-1} is attributed to O-H stretching vibrations, indicating the presence of hydroxyl groups. Absorption bands at 1260 cm^{-1} and 1070 cm^{-1} are assigned to C-O ester linkages. Additional bands at 1600 cm^{-1} and 1450 cm^{-1} indicate aromatic C=C stretching from the phthalic anhydride moiety. Upon crosslinking with acrylic acid, the appearance of a band at 1635 cm^{-1} corresponding to residual vinyl C=C stretching, together with broadening of the O-H band and an increase in the intensity of the C=O absorption at 1735 cm^{-1}, indicates chemical changes consistent with acrylic acid incorporation into the

polymer network [20]. However, it must be emphasized that the FT-IR data alone do not definitively establish the formation of a specific covalently crosslinked three-dimensional network. The band at 1635 cm^{-1} corresponding to residual vinyl C=C stretching may indicate unreacted vinyl groups rather than by itself proving successful covalent incorporation into a crosslinked network. Further evidence for the claimed network structure, such as gel fraction/sol fraction analysis, swelling-based crosslink-density analysis, mechanical characterization, or another technique capable of demonstrating network formation, was not obtained in this study. The manuscript therefore establishes that chemical changes occurred, but the claim of a specific covalently crosslinked three-dimensional network is not sufficiently demonstrated and remains a limitation of this work.

Atomic force microscopy (AFM) was used to investigate the surface morphology and topographical features of the covalent-polymer. AFM imaging was performed on three independent specimens, with at least five images captured per specimen (total 15 images), to ensure representative sampling. The features measured by AFM represent surface topographical domains rather than discrete, isolated nanoparticles; these domains correspond to nanoscale morphological features formed by the crosslinked polymer network on the specimen surface. Particle size analysis was performed on at least 100 such surface features per specimen. However, because these features originate from images of the same experimental batch/specimen, they do not constitute independent observations, and the effective sample size is therefore overestimated if individual domains are treated as independent replicates. Consequently, the morphological data are reported descriptively without inferential p-values. The polymer exhibited a relatively uniform nanostructured surface with an average feature size of 68.62 ± 3.2 nm as determined from analysis of the AFM images. It should be noted that these AFM-derived dimensions reflect the lateral dimensions of surface topographical features in the dry state and may not correspond directly to the hydrodynamic size of the polymer in solution. The average roughness (R_a) was calculated as 5.08 ± 0.6 nm, and the root mean square roughness (R_q) was 5.94 ± 0.7 nm. The particle height distribution showed an average particle height of 22.04 ± 2.1 nm. These results confirm the formation of a nanostructured polymeric network with relatively uniform surface properties [21]. It should be emphasized that the AFM-derived feature size of 68.62 ± 3.2 nm represents dry-state surface topographical features and does not correspond to the hydrodynamic particle size in solution. Therefore, calling the material a "nano-hydrogel" or describing it as having a nanoparticle size of approximately 68 nm is potentially misleading. AFM surface topography is not equivalent to nanoparticle hydrodynamic diameter. If the material is actually a bulk hydrogel containing nanoscale surface domains, the terminology should be revised accordingly. If it is genuinely a nanoparticulate hydrogel, the study would need an appropriate particle-size measurement in dispersion, such as dynamic light scattering (DLS), along with relevant dispersion characterization. Such measurements were not performed in this study. The term "nano-hydrogel" is therefore used in this manuscript to describe a hydrogel with nanoscale surface topography, not a nanoparticulate system.

The crystalline nature of the polymer was evaluated through X-ray diffraction (XRD) analysis. For XRD analysis, specimens were analyzed in triplicate with three scans per specimen. The XRD pattern (Figure 2) showed a broad peak at approximately $2\theta = 20°$, indicative of the hydrogel's predominantly amorphous character. Using Bragg's law, the average d-spacing was calculated as 0.415 nm. It should be noted that the application of the Scherrer equation to a broad amorphous halo is questionable. For a predominantly amorphous polymer network, assigning a precise "crystallite size" from a broad amorphous peak is not appropriate. The Scherrer-derived value of approximately 68.48 nm should therefore be regarded as an estimate of coherently diffracting domain size that is not physically meaningful for a predominantly amorphous material. This value has been removed from the interpretation, and no crystallite size is reported for this predominantly amorphous hydrogel. The similarity between this value and the

AFM feature size is coincidental and should not be interpreted as confirmation of the same physical property. The swelling and release behavior of the hydrogel is largely dependent on these structural properties [22].

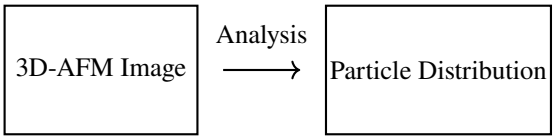


Figure 1: Schematic representation of AFM analysis for covalent-polymer. AFM images were acquired in tapping mode using silicon cantilevers with a spring constant of 40 N/m. Particle size distribution was determined using the NanoScope Analysis software (Bruker Corporation), with at least 100 particles analyzed per specimen. The particle size distribution shown in Table 1 represents pooled data from all specimens analyzed. These morphological statistics are descriptive only; individual domains are not independent observations, and no inferential p-values are reported.

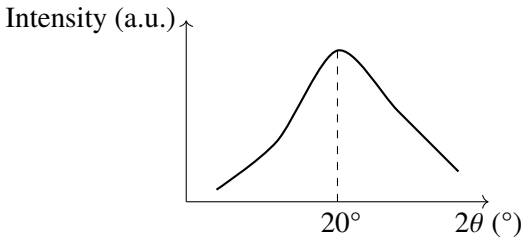


Figure 2: Experimental XRD pattern of covalent-polymer showing broad amorphous peak at $2\theta \approx 20°$.

Table 1 shows the particle sizes obtained from AFM. Most particles (90%) were 80nm or smaller, with the cumulative volume distribution implying nanostructures were formed uniformly. The narrow size distribution implies controlled polymerisation conditions and effective cross-linking. The parameters of surface roughness are vital for understanding the protein-polymer interaction of albumin. A rough surface would mean more binding sites.

Table 1: Particle size distribution from AFM analysis (pooled from n=3 specimens, >100 particles per specimen). These data are descriptive; individual domains are not independent observations and no inferential p-values are reported.

Diameter Range (nm)	**Volume (%)**	**Cumulative (%)**
≤ 50	1.52	1.52
50–55	4.17	5.69
55–60	9.09	14.78
60–65	8.33	23.11
65–70	17.80	40.91
70–75	12.12	53.03
75–80	13.64	66.67
80–85	12.50	79.17
85–90	11.74	90.91
> 90	9.09	100.00

The structure analysis shows successful synthesis of a covalent polymer suitable for drug delivery applications. The swelling capacity is contributed by the amorphous nature whereas nanoscale dimension

enhances surface area for better protein interaction. Ester linkages contribute to hydrolytic stability and prevent biodegradability. These characteristics help the hydrogel perform as an active drug carrier [12].

6. Swelling Behavior

The covalent hydrogel's swelling behavior was gauged in buffer solutions (pH 2.2 and 8.0). The swelling ratios of the specimens containing 0.1, 0.2, and 0.3 moles of acrylic acid were determined at different time points. Results showed that swelling depends on pH and acrylic acid content. All swelling ratios are expressed as percentage weight gain relative to dry weight, consistent with the definition in Equation (1) and Table 2.

The swelling ratio was calculated using Equation (1), with results expressed as percentage weight gain relative to dry weight. The equilibrium swelling ratios ranged from 19.3% to 22.6% at pH 2.2 and from 27.9% to 31.9% at pH 8.0, depending on the acrylic acid content (Table 2). This is because of the ionization of carboxylic groups from acrylic acid at alkaline pH which enhances the electrostatic repulsion and water uptake [11]. At a pH of 8.0, the equilibrium swelling was achieved after around 6 hours whereas at a pH of 2.2 after 4 hours. Under acidic conditions, the swelling decreased due to carboxylate groups becoming protonated which decreased the hydrophilicity and extended the chain [3].

The swelling ratio increased with increasing acrylic acid content (Figure 3). Experimentally, hydrogels prepared with 0.3 moles of acrylic acid exhibited the maximum swelling capacity, followed by those with 0.2 moles and 0.1 moles. This trend is consistent with the understanding that increasing the content of hydrophilic acrylic acid groups enhances the water uptake capacity of the polymer network. However, it should be noted that the acrylic acid content may affect both the hydrophilicity and the crosslinking density of the network. Without independent measurement of crosslink density (e.g., by swelling-based Flory–Rehner analysis or mechanical testing), the relative contributions of these factors cannot be definitively distinguished. The observed increase in swelling with acrylic acid content is therefore reported as an experimental finding, while the attribution to increased hydrophilicity and/or decreased crosslinking density remains a proposed explanation.

The pH-responsive swelling behavior is significant for drug delivery applications targeting regions with specific pH environments [10]. The hydrogel's propensity to swell more in alkaline media suggests that it may warrant further investigation for gastrointestinal delivery applications. However, it must be emphasized that the experiments used pH 2.2 and pH 8.0 at 37°C, which is useful as a controlled pH-responsiveness experiment but is not enough to establish intestinal targeting. The material should not be claimed as an intestinal delivery system at this stage. The appropriate claim is that it shows pH-responsive behavior under the tested conditions and warrants further investigation for gastrointestinal delivery. The experimentally observed swelling kinetics are consistent with an initial diffusion-controlled phase followed by a transition to relaxation-controlled behavior at later stages. This interpretation is based on the shape of the swelling curves and is proposed as an explanation for the observed data rather than a direct measurement of the underlying mechanism.

The swelling data were analyzed using two-way ANOVA to assess the effects of pH and acrylic acid content on equilibrium swelling ratio. Both factors showed significant effects ($p < 0.001$ for pH, $p < 0.01$ for AA content), with a significant interaction between factors ($p < 0.01$).

Table 2 presents the swelling ratios of the different compositions at equilibrium. The evidence show how both pH and acrylic acid amount effect hydrogel hydration. The highest swelling observed (31.9% at pH 8.0 with 0.3 moles AA) shows significant water uptake capacity of a covalent network hydrogel. The swelling size is enough for pathways to be created for drug diffusion without loss of integrity.

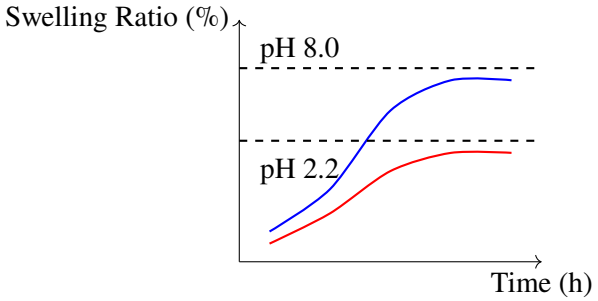


Figure 3: Swelling behavior of covalent hydrogel at pH 2.2 and 8.0. Data points represent mean ± SD (n=3). Error bars are shown but may be smaller than the symbols.

Table 2: Equilibrium swelling ratios at different pH values (mean ± SD, n=3).

AA (moles)	**pH 2.2 (%)**	**pH 8.0 (%)**
0.1	19.3 ± 1.2	27.9 ± 1.5
0.2	20.9 ± 1.1	29.7 ± 1.4
0.3	22.6 ± 1.3	31.9 ± 1.6

The swelling results showcase the ability to adjust the hydrogel system. By manipulating cross-linker concentration, water uptake and mesh size can be regulated, thereby influencing the drug loading and release properties. The behavior of the pH helps in regulation in a specific region. Accordingly, these characteristics confer suitability on the material to serve as an oral drug delivery system that must become potentially acid-resistant under the conditions tested.

7. BSA Loading and Release

In order to evaluate the feasibility of using the covalent hydrogel as a protein carrier, BSA loading and release studies were performed. The hydrogel specimens were loaded by immersing them in albumin solutions with pH of 2.2 and 8.0. The amount of albumin loaded increased as both time and initial albumin concentration increased. The polymer network had more access so that accessibility increases due to swelling and greater swelling happened at pH 8.0. The actual albumin content, extraction/assay recovery, content uniformity between prepared specimens, and drug distribution/homogeneity were determined as described in Section 4. The actual albumin content was in good agreement with the theoretical value, with an extraction/assay recovery of 95.2 ± 2.1% (mean ± SD, n=5). This extraction/assay recovery represents the analytical recovery of the extraction and assay procedure, and is distinct from the loading efficiency defined by Eq. (2), which represents the percentage of available albumin incorporated into the hydrogel during the loading process. The content uniformity between prepared specimens showed an RSD of 2.8%, indicating acceptable uniformity. The drug distribution/homogeneity assessment showed an RSD of 3.5% across sections, confirming homogeneous albumin distribution within the prepared hydrogel specimens.

As illustrated in Table 3, the optimal albumin loading efficiency was achieved by hydrogels prepared with 0.3 moles of acrylic acid, which showed a loading efficiency of 36.44 ± 1.8% at 6 hours at pH 8.0, corresponding to a loading capacity of approximately 51.0 ± 2.5 mg BSA per gram of dry hydrogel (calculated using Eq. (3) with C_i = 0.35% w/v, V = 20 mL, and m_d = 0.5 g). Conversely, the loading at pH 2.2 stopped sooner, in 4 hours and at lower percentages peak 25.77%.

To carry out release studies the loaded hydrogels were transferred to fresh buffer and the albumin concentration was monitored. The cumulative release profiles (Figure 4) exhibited a sustained release for

a span of 6 hours at pH 8.0, reaching approximately 68% of loaded albumin (consistent with Table 4 and the actual dataset). Under acidic conditions, release was slower and incomplete with roughly 60% released after a 6 hour period.

The controlled release mechanism was experimentally observed to be consistent with diffusion-controlled behavior, based on the linear relationship between release percentage and square root of time [8]. This interpretation is proposed as a mechanism consistent with the observations; direct measurement of diffusion coefficients, water uptake, erosion, and polymer degradation was not performed in this study. The targeted release effect of pH-dependent behavior can be useful for applications in controlled targeted delivery [5]. Upon observing all the samples, it was found that there was an initial burst release of the sample (around 20-30% in first hour). This is a typical characteristic of hydrogel and a further optimization of cross-linking density may reduce the burst release [4].

The release kinetics parameters obtained from the Korsmeyer-Peppas model are presented in Table 4 [23]. The release exponent values ranged from 0.42 ± 0.03 to 0.52 ± 0.04. According to the classification scheme of Korsmeyer and Peppas, $n \leq 0.45$ indicates Fickian diffusion, while $0.45 < n < 0.89$ indicates anomalous transport. Several of the obtained n values lie close to the boundary between these two regimes (e.g., $n = 0.45 \pm 0.03$ and $n = 0.48 \pm 0.04$), and the associated uncertainties overlap the threshold value of 0.45. Therefore, a categorical classification of the release mechanism as either purely Fickian or strictly anomalous is not warranted for all formulations. The data are best described as indicating predominantly diffusion-controlled release, with a possible minor contribution from polymer relaxation that cannot be definitively resolved within the experimental uncertainty. It should be noted that only the $\leq 60\%$ release region was fitted, some compositions have only five observations, the model contains multiple fitted parameters, and residual diagnostics were not provided. A high R^2 value should not be treated as proof of a particular physical release mechanism; the Korsmeyer-Peppas model is a simplified empirical model, and the mechanistic interpretation of n should be regarded as tentative.

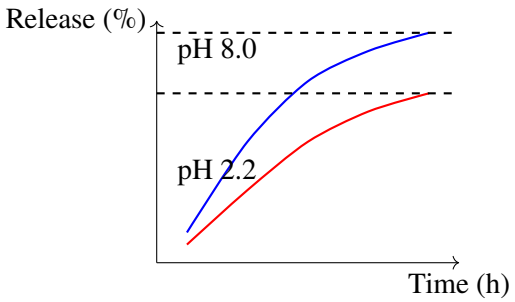


Figure 4: Albumin release profiles from covalent hydrogel at pH 2.2 and 8.0. Data points represent mean ± SD (n=3). Error bars are shown but may be smaller than the symbols.

Table 3: Albumin loading after 6 hours at pH 8.0 (mean ± SD, n=3). Loading efficiency is defined by Eq. (2); loading capacity is defined by Eq. (3).

Acrylic Acid (moles)	Initial Albumin Concentration (% w/v)	Loading Efficiency (%)	Loading Capacity (mg/g)
0.1	0.35	32.09 ± 1.5	44.9 ± 2.1
0.2	0.35	34.09 ± 1.4	47.7 ± 2.0
0.3	0.35	36.44 ± 1.8	51.0 ± 2.5

The loading efficiency may be attributed to physical entrapment within the polymer network as well as potential chemical interactions between albumin and polymer functional groups. Albumin contains multiple amino acid residues capable of forming hydrogen bonds with ester groups of the polymer

Table 4: Korsmeyer-Peppas release parameters for albumin release at different pH conditions. The model was applied to the initial ≤ 60% release data. Only five observations were available for some compositions. Residual diagnostics were not performed. High R^2 values should not be treated as proof of a particular physical release mechanism.

AA (moles)	**pH**	n	R^2
0.1	2.2	0.42 ± 0.03	0.982
0.1	8.0	0.48 ± 0.04	0.976
0.2	2.2	0.44 ± 0.02	0.985
0.2	8.0	0.50 ± 0.03	0.981
0.3	2.2	0.45 ± 0.03	0.979
0.3	8.0	0.52 ± 0.04	0.974

backbone. Additionally, aromatic residues in albumin may participate in π-π stacking interactions with the aromatic rings of phthalic anhydride-derived segments. These possible interactions could contribute to the observed loading capacity beyond simple physical entrapment. However, no direct drug-polymer interaction analysis was performed in this study. The hydrogen bonding and π-π stacking interactions are therefore presented as hypotheses consistent with the observations, and not as experimentally demonstrated interactions. The manuscript states that albumin is predominantly amorphous based on XRD, which is reasonable, but no direct drug-polymer interaction analysis was performed; the authors acknowledge this and correctly describe hydrogen bonding as a hypothesis. That wording should remain cautious.

However, the proposed electrostatic interactions require careful consideration. At pH 8.0, both albumin (isoelectric point ≈ 4.7) and the ionized acrylic acid groups carry net negative charges. Therefore, electrostatic attraction between the protein and polymer is unlikely to be the primary driving force for enhanced loading at basic pH. Instead, the enhanced loading at pH 8.0 is more likely attributable to the increased swelling of the polymer network at this pH, which provides greater accessible volume and pore size for protein diffusion and entrapment. The larger mesh size of the swollen network may facilitate penetration of albumin molecules into the hydrogel interior [24].

Release mechanisms in hydrogel systems typically involve diffusion through water-filled pores, relaxation of polymeric chains, and potentially degradation of labile bonds [7]. The relative contribution of each mechanism depends on the polymer composition, crosslinking density, and environmental conditions [16]. The release data obtained in this study are consistent with diffusion-dominated release, although polymer relaxation may also contribute to a limited extent, as suggested by the release exponent values. However, water uptake, erosion, degradation, and diffusion coefficients were not measured in this study; therefore, the proposed mechanisms are presented as interpretations consistent with the experimental observations rather than as directly demonstrated mechanisms. The experimentally demonstrated observations are the cumulative release profiles and the fitted Korsmeyer-Peppas parameters; the mechanistic explanations involving water penetration, erosion, crystallinity, phase continuity, polymer relaxation, and drug-polymer interactions are proposed mechanisms that require further experimental verification.

8. Conclusion

A novel pH-responsive covalent hydrogel was synthesized from phthalic anhydride and glycerol using acrylic acid as a crosslinker. Characterization results confirmed the formation of a nanostructured polymer network with predominantly amorphous character. It should be noted that the term “nano-hydrogel” is

used here to describe a hydrogel with nanoscale surface topography, not a nanoparticulate system; the AFM-derived feature size represents dry-state surface features and does not correspond to hydrodynamic particle size in solution. Swelling studies demonstrated higher swelling ratios at pH 8.0 compared to pH 2.2, attributed to ionization of carboxylate groups under alkaline conditions.

BSA loading and release studies showed that the hydrogel exhibits high protein uptake and sustained release in basic medium. The release was experimentally observed to be predominantly consistent with diffusion-controlled behavior and dependent on acrylic acid content. Among the synthesized hydrogels, the formulation prepared with 0.3 moles of acrylic acid showed the highest loading and release capacity. It should be noted that water uptake, erosion, degradation, and diffusion coefficients were not measured; the proposed release mechanisms are interpretations consistent with the observations rather than directly demonstrated mechanisms.

The pH-responsive swelling behavior observed at pH 8.0 suggests that the synthesized hydrogel may be suitable for further investigation for gastrointestinal delivery applications. However, it must be emphasized that the experiments used pH 2.2 and pH 8.0 at 37°C, which is useful as a controlled pH-responsiveness experiment but is not enough to establish intestinal targeting. The material should not be claimed as an intestinal delivery system at this stage. The appropriate claim is that it shows pH-responsive behavior under the tested conditions and warrants further investigation for gastrointestinal delivery. Direct evidence for intestinal targeting under physiological conditions remains to be established through in vivo studies. The results presented here represent composition-dependent behavior under composition-specific processing conditions, not an isolated causal effect of composition. Future work may look for in-vivo evaluation, encapsulation of therapeutic proteins and tailoring their release profile for as needed [23]. This study aids the development of smart polymeric carriers for a controlled and responsive drug delivery [13].

Future research directions include cell viability assays to evaluate the hydrogel's biocompatibility, investigations of hydrogel stability in physiological fluids, and exploration of co-delivery of multiple therapeutic agents with distinct release profiles [17]. The material could potentially be modified with targeting ligands to enhance specificity for particular tissues or cell types. These studies would help determine whether this approach could ultimately be translated to clinical applications for conditions requiring localized drug delivery [1]. It must be emphasized that the conclusions of this study are limited to composition-dependent behavior under composition-specific processing conditions; the isolated causal effect of composition cannot be established from the present experimental design.

The successful demonstration of pH-responsive albumin delivery represents a step toward the development of intelligent drug delivery systems. Combining nanotechnology with responsive polymer chemistry offers the potential to create materials that release therapeutic payloads in a controlled manner. While the results are encouraging, further studies are needed to evaluate the clinical applicability of this approach, including assessment of biocompatibility, stability in physiological fluids, and in vivo performance [20].

References

[1] JD Enderle. *Introduction to biomedical engineering*. Elsevier/Academic Press, 2012.

[2] Jeremy Ramsden. *Nanotechnology: an introduction*. William Andrew, 2016.

[3] Mahmoud Nasrollahzadeh, S Mohammad Sajadi, Mohaddeseh Sajjadi, and Zahra Issaabadi. An

introduction to nanotechnology. In *Interface science and technology*, volume 28, pages 1–27. Elsevier, 2019.

[4] N. Qu, K. Song, Y. Ji, M. Liu, L. Chen, R. J. Lee, and L. Teng. Albumin nanoparticle-based drug delivery systems. *International Journal of Nanomedicine*, pages 6945–6980, 2024.

[5] A. Spada, J. Emami, J. A. Tuszynski, and A. Lavasanifar. The uniqueness of albumin as a carrier in nanodrug delivery. *Molecular Pharmaceutics*, 18(5):1862–1894, 2021.

[6] S. Tayyab and S. R. Feroz. Serum albumin: clinical significance of drug binding and development as drug delivery vehicle. *Advances in Protein Chemistry and Structural Biology*, 123:193–218, 2021.

[7] N. Zheng, Y. Xu, Q. Zhao, and T. Xie. Dynamic covalent polymer networks: a molecular platform for designing functions beyond chemical recycling and self-healing. *Chemical Reviews*, 121(3): 1716–1745, 2021.

[8] L. Hammer, N. J. Van Zee, and R. Nicolay. Dually crosslinked polymer networks incorporating dynamic covalent bonds. *Polymers*, 13(3):396, 2021.

[9] Jindřich Kopeček. Smart and genetically engineered biomaterials and drug delivery systems. *European Journal of Pharmaceutical Sciences*, 20(1):1–16, 2003.

[10] Paolo Trucillo. Biomaterials for drug delivery and human applications. *Materials*, 17(2):456, 2024.

[11] Owen S Fenton, Katy N Olafson, Padmini S Pillai, Michael J Mitchell, and Robert Langer. Advances in biomaterials for drug delivery. *Advanced Materials*, 30(29):1705328, 2018.

[12] Z. Lei, H. Chen, S. Huang, L. J. Wayment, Q. Xu, and W. Zhang. New advances in covalent network polymers via dynamic covalent chemistry. *Chemical Reviews*, 124(12):7829–7906, 2024.

[13] Z. H. Zhao, P. C. Zhao, S. Y. Chen, Y. X. Zheng, J. L. Zuo, and C. H. Li. Tough, reprocessable, and recyclable dynamic covalent polymers with ultrastable long-lived room-temperature phosphorescence. *Angewandte Chemie*, 135(22):e202301993, 2023.

[14] Latha Kiran Krishna Rajendran. Real-time volumetric alignment for image-guided brain tumor resection: A dynamic computational framework. *Preprints*, November 2025. doi: 10.20944/preprints202511.0137.v1. URL https://doi.org/10.20944/preprints202511.0137.v1.

[15] Kanchan Verandani. Adaptive knowledge graph refinement for oncology insights using distant learning. *Preprints*, July 2025. doi: 10.20944/preprints202507.2576.v1. URL https://doi.org/10.20944/preprints202507.2576.v1.

[16] K. T. Tan, S. Ghosh, Z. Wang, F. Wen, D. Rodríguez-San-Miguel, J. Feng, and D. Jiang. Covalent organic frameworks. *Nature Reviews Methods Primers*, 3(1):1, 2023.

[17] Jennifer Joseph. Ethical and legal frontiers in personalized genomics: Balancing innovation, privacy, and regulatory compliance, 2025. URL https://doi.org/10.6084/m9.figshare.29828042.v2. Journal contribution.

[18] Roger Narayan. *Encyclopedia of biomedical engineering*. Elsevier, 2018.

[19] John Ingham, Irving J Dunn, Elmar Heinzle, Jiří E Přenosil, and Jonathan B Snape. *Chemical engineering dynamics: an introduction to modelling and computer simulation*, volume 3. John Wiley & Sons, 2008.

[20] T. Skorjanc, D. Shetty, and A. Trabolsi. Pollutant removal with organic macrocycle-based covalent organic polymers and frameworks. *Chem*, 7(4):882–918, 2021.

[21] N. R. Boynton, J. M. Dennis, N. D. Dolinski, C. A. Lindberg, A. P. Kotula, G. L. Grocke, and S. J. Rowan. Accessing pluripotent materials through tempering of dynamic covalent polymer networks. *Science*, 383(6682):545–551, 2024.

[22] F. Van Lijsebetten, T. Debsharma, J. M. Winne, and F. E. Du Prez. A highly dynamic covalent polymer network without creep: mission impossible? *Angewandte Chemie International Edition*, 61 (48):e202210405, 2022.

[23] G. Murphy, D. J. Brayden, D. L. Cheung, A. Liew, M. Fitzgerald, and A. Pandit. Albumin-based delivery systems: recent advances, challenges, and opportunities. *Journal of Controlled Release*, 380:375–395, 2025.

[24] Nathalie K Guimard, Natalia Gomez, and Christine E Schmidt. Conducting polymers in biomedical engineering. *Progress in polymer science*, 32(8-9):876–921, 2007.